Generalized Frequency Domain Formulation of the Switching Frequency for Hysteresis Current Controlled VSI Used for Load Compensation

Rajesh Gupta, *Senior Member, IEEE*

***Abstract*—In this paper, a generalized frequency domain method is proposed to obtain the switching frequency formulation for hysteresis current controlled voltage source inverter (VSI)-based shunt compensator. The formulation obtained from the high-frequency model based on the Tsypkin's method explicitly shows the relation between the maximum switching frequency with the system and design parameters. The shunt compensator has been used for the load compensation in a distribution system for both weak and strong feeder supplying a nonlinear load. The maximum switching frequency has been shown related with hysteresis bandwidth and parameters of the VSI, feeder, and load of the distribution system. It is shown that the feeder and load reactance has a significant effect in determining the maximum switching frequency for the weak feeder distribution systems. However, the maximum switching frequency is mainly dependent upon the shunt compensator parameters for strong feeder distribution systems. The minimum switching frequency in general depends upon the modulation depth of the VSI. The results are verified using as power systems CAD (PSCAD) simulation studies for single-phase load compensation. A laboratory model distribution system has been used for the experimental verification.**

***Index Terms*—Hysteresis current control, modulation depth, nonlinear load, switching frequency, Tsypkin's method.**

I. Introduction

NEED to estimate the switching frequency of the power switching devices is an important design requirement for high-power voltage source inverter (VSI) applications [1]. This is mainly required for proper planning of the thermal management and cooling of the converters [2]. Commonly used hysteresis current control method for the two-level VSI is very popular due to its simplicity, good dynamic performance, and robustness properties [3]–[8]. However, it suffers from the disadvantage of variable switching frequency over the fundamental frequency cycle. The switching frequency also varies with the system and controller parameters [7]. For the hysteresis control applications, it is important to know the maximum switching frequency as it leads to the better estimate of the maximum switching loss in the VSI [9], [10]. In general, the estimation of switching frequency for hysteresis current control operation of the VSI is important due to the following reasons: 1) estimation of inverter switching loss; 2) limiting the switching frequency within the ratings of the switches; 3) determination of ripple amplitude; 4) design of switching ripple filter; 5) estimation of voltage and current harmonic distortions.

The formulation of switching frequency for the hysteresis current control application means to find out the relationship of the switching frequency of the switching devices of the VSI with various system and design parameters [11]–[14]. For distribution system compensation application [15], these parameters include distribution system feeder impedance, supply voltage, VSI passive filters, dc-link voltage, load parameters, controller design parameters, and hysteresis bandwidth.

Conventionally, the relationship between the switching frequency and hysteresis bandwidth is obtained based on the time-domain slope method for the hysteresis current control applications [16]–[18]. In [16], the derivations are obtained for the current control in drives applications. In [17], the results are obtained for the distribution system compensation using shunt compensator. In [18], the time-domain method is further explored and it is shown that for the current control application the reduction in switching frequency from its maximum value at other instants of time depends upon the modulation depth of the VSI. For load compensation, this depends upon the factors such as supply voltage, load parameters, reference current, etc.

The relation between the switching frequency and hysteresis bandwidth becomes complicated in case the shunt compensator is used in a weak feeder distribution system such that it has high feeder impedance. This complexity further grows if the reference current is actually derived from the load current, which also carries switching components [19]. It is difficult to use time-domain method for generalized formulation of the switching frequency. In the literature, the switching frequency formulation has been obtained only for the strong feeder distribution system based on the time-domain approach [11], [17].

Recently, the method of Tsypkin's has been used for generalized frequency domain characterization for the sliding mode controlled two-level and three-level inverter based on hysteresis modulation [7]. The method is further extended for the switching characterization of the multiband hysteresis modulation of the cascaded multilevel inverter in [20]. The basic Tsypkin's method for hysteresis-based relay control system can be seen in [21]–[23]. Recently, the hysteresis modulation has been used

Manuscript received February 15, 2011; revised May 7, 2011 and August 1, 2011; accepted November 2, 2011. Date of current version February 27, 2012. This work was supported in part by the Research and Consultancy Cell, Motilal Nehru National Institute of Technology Allahabad, India, through the project titled "Design of intelligent power modules for multilevel inverters used as power converter for PV solar panel." Recommended for publication by Associate Editor P. Rodriguez.

The author is with the Department of Electrical Engineering, Motilal Nehru National Institute of Technology, Allahabad 211004, Uttar Pradesh, India (e-mail: rajeshgupta310@rediffmail.com).

Digital Object Identifier 10.1109/TPEL.2011.2175750

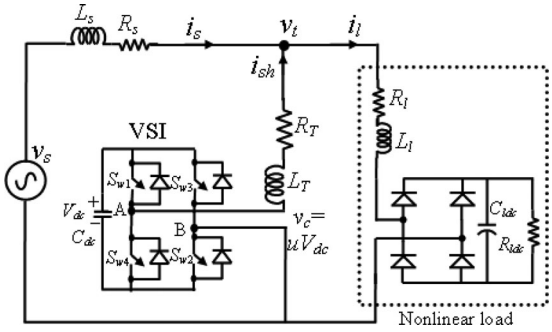

Fig. 1. Single-phase model of a shunt compensated distribution system.

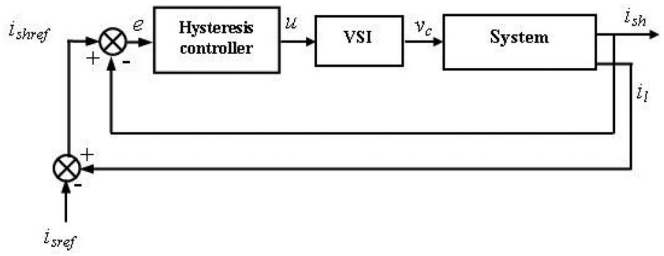

Fig. 2. Block diagram of load compensation.

for the control of the multilevel inverters using multiple hysteresis bands [20], [24]–[26].

In this paper, a generalized frequency domain formulation has been developed based on Tsypkin's method, to find out the relation between the maximum switching frequency and hysteresis bandwidth and with rest of the system parameters for current controlled two-level VSI-based application. The current control application has been considered for load compensation in both weak and strong feeder distribution system supplying a nonlinear load. The results are derived using the transfer function of the shunt compensated distribution system and subsequently obtained high-frequency model. The effect of modulation depth on minimum switching frequency has been shown through the variations in the supply voltage and the load in the distribution system. The detailed simulation studies have been performed to verify the results for a single-phase distribution system. Experimental verification of the results has been obtained using the laboratory model of the distribution system.

The generalized formulation of the switching frequency proposed in this paper can easily be extended for the perphase analysis of the three-phase four-wire distribution system load compensation [7], [27] and for multiband hysteresis current control application with cascaded multilevel inverters [20], [24]. In addition, the proposed method can easily be used to derive the formulation of the switching frequency for any other VSI-based application controlled through the hysteresis modulation.

II. Modeling of Shunt Compensator

A shunt compensator used for load compensation tracks the reference shunt current in order to eliminate the harmonic contents of the nonlinear load and to mitigate the poor load power factor [11], [19], [24]. Fig. 1 shows the single-phase model of the shunt compensated distribution system. The distribution system is supplied from the voltage source v_s through the feeder inductance L_s and resistance R_s. The shunt compensator consists of a VSI, an interfacing inductance L_T, and a resistance R_T. Here, an H-bridge is considered for single-phase two-level VSI. Each of the switches Sw_1 to Sw_4 in the H-bridge consists of the power semiconductor devices such as insulated gate bipolar transistor (IGBT) and antiparallel diode. The voltage $V_{\rm dc}$ represents the dc-link voltage of the VSI supported by the dc-link capacitor $C_{\rm dc}$. The currents flowing through the different branches are the source current i_s, the load current i_l, and the shunt current $i_{\rm sh}$. The net controllable voltage v_c at the output of the VSI is $uV_{\rm dc}$, where u is defined as the control input and represents the switching logic of the VSI, i.e., $+1$ and -1, for the two-level case considered here.

The nonlinear load considered in this paper is assumed to be a bridge rectifier with input impedance (L_l, R_l) and connected to the distribution system at the point of common coupling (PCC). For a single-phase load, the output dc voltage of the bridge rectifier is fed to a resistive load $R_{\rm ldc}$ supported by a parallel dc capacitor $C_{\rm ldc}$. This nonlinear load is called as a voltage source type [7], [27]–[29] and represents many domestic and industrial nonlinear loads. It can be modeled by a harmonic perturbation voltage source v_d, where v_d is the Thevenin equivalent voltage source of such load. The input impedance (L_l, R_l) of this load approximately represents its Thevenin equivalent impedance. The state-space model of the system with three inputs v_s, u, and v_d, and the output $i_{\rm sh}$ can be derived by considering the state vector $x = [i_{\rm sh}\ i_l]^T$ as [19]

$$\begin{aligned} \dot{x} &= Ax + b_1 v_s + b_2 u + b_3 v_d \\ i_{\rm sh} &= cx \end{aligned} \tag{1}$$

where $c = [1\ 0]$ and

$$A = \frac{1}{L_{\rm eq}^2} \times \begin{bmatrix} -(R_T L_s + R_T L_l + R_s L_l) & (R_s L_l - R_l L_s) \\ (L_T R_s - L_s R_T) & -(R_s L_T + R_l L_T + L_s R_l) \end{bmatrix}$$

$$b_1 = \frac{1}{L_{\rm eq}^2}\begin{bmatrix} -L_l \\ L_T \end{bmatrix}, \qquad b_2 = \frac{1}{L_{\rm eq}^2}\begin{bmatrix} (L_s + L_l)V_{\rm dc} \\ L_s V_{\rm dc} \end{bmatrix},$$

$$b_3 = \frac{1}{L_{\rm eq}^2}\begin{bmatrix} L_l \\ -L_T \end{bmatrix}, \quad L_{\rm eq}^2 = L_T L_s + L_l L_T + L_l L_s.$$

For load compensation using hysteresis current controller with the VSI, the shunt compensator follows the block diagram shown in Fig. 2. The reference shunt current $i_{\rm shref}$ is generated after subtracting the reference source current $i_{\rm sref}$ from the actual load current i_l [19], and will be discussed in detail in Section VI.

Following transfer functions can be defined from (1) as $G_{ui_{\rm sh}}(s) = i_{\rm sh}(s)/u(s)|_{v_s=0, v_d=0}$ and $G_{ui_l}(s) = i_l(s)/u(s)|_{v_s=0, v_d=0}$.

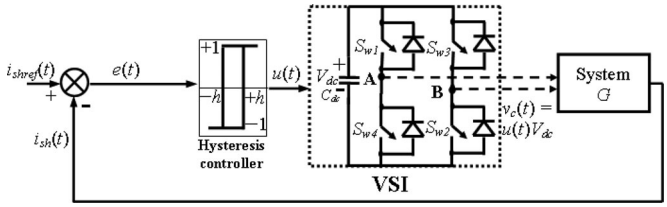

Fig. 3. Block diagram of hysteresis current controlled VSI for shunt compensator.

These transfer functions can be derived as follows:

$$G_{ui_{\rm sh}}(s) = \left.\frac{i_{\rm sh}(s)}{u(s)}\right|_{v_s=0, v_d=0} = \left(\frac{V_{\rm dc}}{L_{\rm eq}^2}\right)\frac{(L_s+L_l)s+(R_s+R_l)}{D(s)} \quad (2)$$

$$G_{ui_l}(s) = \left.\frac{i_l(s)}{u(s)}\right|_{v_s=0, v_d=0} = \left(\frac{V_{\rm dc}}{L_{\rm eq}^2}\right)\frac{L_s s+R_s}{D(s)} \quad (3)$$

where $D(s) = s^2 + D_1 s + D_2$

$$D_1 = \frac{L_T(R_s+R_l)+L_s(R_l+R_f)+L_l(R_f+R_s)}{L_{\rm eq}^2}$$

$$D_2 = \frac{R_{\rm eq}^2}{L_{\rm eq}^2}$$

and $R_{\rm eq}^2 = R_T R_s + R_l R_T + R_l R_s$.

III. Hysteresis Current Control

Block diagram of the hysteresis current controlled VSI for the shunt compensator is shown in Fig. 3. The block diagram only shows the inner control loop of Fig. 2. The reference shunt current $i_{\rm shref}$ is compared with the actual shunt current $i_{\rm sh}$ to produce the error $e = (i_{\rm shref} - i_{\rm sh})$. Based upon the value of error e, the hysteresis current controller generates the control input u to drive the single-phase VSI, which in turn control the system G.

The two-level hysteresis controller follows the control law as defined below:

$$u(t) = +1 \quad \text{for } e(t) > +h \quad (4a)$$

$$u(t) = -1 \quad \text{for } e(t) < -h \quad (4b)$$

where h is a suitable hysteresis bandwidth to be chosen depending upon the requirement of the switching frequency of the switching devices used in the VSI.

Consider the H-bridge as shown in Fig. 3 for the two-level inverter modulation. Using (4), the H-bridge VSI is operated under bipolar modulation with two logic levels in u, i.e., $+1$ and -1. The switches S_{w1}, S_{w2} and S_{w3}, S_{w4} in Fig. 3 are operated in pair as follows:

S_{w1} and S_{w2} are ON for $u(t) = +1$ such that $v_c(t) = +V_{\rm dc}$ (5a)

S_{w3} and S_{w4} are ON for $u(t) = -1$ such that $v_c(t) = -V_{\rm dc}$. (5b)

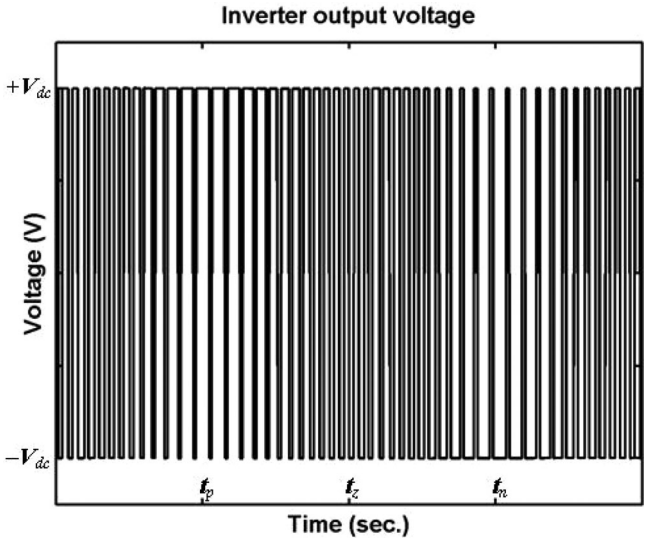

Fig. 4. Output voltage of the H-bridge VSI for two-level hysteresis current control operation.

The instantaneous value of the switching frequency f_i of the switches depends upon the hysteresis bandwidth h, system parameters, and operating conditions. The operating condition changes with the change in load and the change in supply voltage of the distribution system. The VSI output voltage v_c will take on values $+V_{\rm dc}$ and $-V_{\rm dc}$ as shown in Fig. 4 for one cycle of the fundamental frequency f_o. It is assumed that the hysteresis bandwidth h is sufficiently small such that the frequency of switching reversal is fast enough as compared to the fundamental period. Under this condition, the shunt current $i_{\rm sh}$ will track the reference $i_{\rm shref}$ with variable switching frequency of the pair of switches S_{w1}, S_{w2} and S_{w3}, S_{w4} that is reflected in the switching reversal of the VSI output voltage as shown in Fig. 4. This reversal of the output voltage for two-level output takes place at the switching frequency f_i of the switches as shown in Fig. 4. Therefore, the switching harmonics present in the inverter output voltage v_c is directly related to the switching frequency f_i. The two-level output voltage contains low-frequency components (generally at fundamental frequency f_o and its low-order harmonics) and high-frequency pulsed signal corresponding to the switching of the inverter at the frequency f_i. As seen from Fig. 4, the switching frequency with hysteresis current control is variable over one fundamental cycle.

IV. Steady-State Analysis Using Tsypkin's Method

Under steady state, both u and v_c are periodic, containing low-frequency fundamental component and its low-order harmonics, and high-frequency switching components as discussed earlier. Let us consider the control input u ($u = v_c/V_{\rm dc}$) where it undergoes the zero crossing of its low-frequency component (instant t_z in Fig. 4), such that the average of the two-level pulsed output is zero at these instants. Therefore, these pulses assume square wave-shape (i.e., both positive and negative durations are equal). The inverter undergoes maximum switching frequency $f_{i\max}$ near these instants. The inverter undergoes

minimum switching frequency $f_{i\,\min}$ near the instants of positive peak (t_p) and negative peak (t_n), in Fig. 4. It is assumed that the instantaneous switching frequency f_i is significantly higher as compared to the fundamental frequency f_o.

Now let us define a net forward transfer function $G_u(s)$ as follows:

$$G_u(s) = \frac{i_{\rm sh}(s)}{u(s)} = \frac{i_{\rm sh}(s)}{v_c(s)}\frac{v_c(s)}{u(s)} = V_{\rm dc}G(s) \tag{6}$$

where the dc-link voltage $V_{\rm dc}$ appear as a forward gain in Fig. 3 and included with $G(s)$ in (6) to obtain the net forward transfer function $G_u(s)$. This transfer function can also include any other transfer function used in the forward path in Fig. 3, e.g., any linear controller transfer function, zero-order hold transfer function representing sample delay [27], etc. In this paper, the linear controller is considered unity gain and computation time is considered very small such that the sample delay is neglected for simplicity.

It has been shown in [7], [20] that using Tsypkin's analysis, following relationship exists between maximum switching frequency $f_{i\,\max}$ ($=\omega_{i\,\max}/2\pi$) and hysteresis bandwidth h

$$h = -{\rm Im}\left(H_t\left(\omega_{i\,\max}\right)\right) \tag{7}$$

where

$${\rm Im}\{H_t(\omega)\} = \frac{4}{\pi}\sum_{n=1,3,5\ldots}^{\infty}\frac{1}{n}{\rm Im}\left\{G_u\left(jn\omega\right)\right\} \tag{8}$$

where n is the index assuming only odd integers and represents the odd harmonic order of the maximum switching frequency $f_{i\,\max}$ of the square wave shape of the pulse width modulation output near the instant t_z in Fig. 4.

V. High-Frequency Modeling and Formulation of Switching Frequency

In load compensation application shown in Fig. 2, the affect of high-frequency switching ripple in the error function e appears both due to the shunt current feedback $i_{\rm sh}$ and the load current feedback i_l. Since (8) has been derived based on the switching ripple feedback; therefore, the following net transfer function G_u in (8) for the switching characterization should be used

$$G_u(s) = \left[G_{ui_{\rm sh}}(s) - G_{ui_l}(s)\right] \tag{9}$$

where $G_{ui_{\rm sh}}(s)$ and $G_{ui_l}(s)$ are obtained in (2) and (3), respectively. The transfer function $G_{ui_{\rm sh}}(s)$ appear as a forward path transfer function for the shunt current control loop in Fig. 2. Since the load current switching ripples appear in opposite sign to that of the shunt current, therefore, $G_{ui_l}(s)$ is included with $G_{ui_{\rm sh}}(s)$ with negative sign in $G_u(s)$ for high-frequency analysis. There is no contribution of switching ripple due to reference source current $i_{\rm sref}$ in Fig. 2 as it is a computed quantity. The following frequency domain transfer function can be derived after substituting $G_{ui_{\rm sh}}(s)$ and $G_{ui_l}(s)$ from (2) and (3), respectively, in (9)

$$G_u(j\omega) = \left(\frac{V_{\rm dc}}{L_{\rm eq}^2}\right)\frac{j\omega L_l + R_l}{D\left(j\omega\right)}. \tag{10}$$

The approximate high-frequency model can be obtained by substituting $\omega = \omega_h$ in (10) and letting $\omega_h \to \infty$ as follows:

$${\rm Im}\left(G_u\left(j\omega_h\right)\right) \approx -\frac{V_{\rm dc}}{L_T + L_s + \left(L_T L_s/L_l\right)}\frac{1}{\omega_h}. \tag{11}$$

The relation between the hysteresis bandwidth h required for the maximum switching frequency $f_{i\,\max}$ can be obtained using (7). The relation is derived based on the high-frequency model obtained in (11). Consider the following approximation of π-series [30], [31]

$$\frac{\pi^2}{8} = 1 + \frac{1}{3^2} + \frac{1}{5^2} + \cdots = \sum_{n=1,3,5,\ldots}^{\infty}\frac{1}{n^2}. \tag{12}$$

Substituting (11) in (8) and then making use of (12), the expression of ${\rm Im}\left\{H_t\left(\omega_{i\,\max}\right)\right\} = -\left(\pi V_{\rm dc}\right)/\left(2\omega_{i\,\max}\left(L_T + L_s + L_T L_s/L_l\right)\right)$ can be obtained. Again substituting ${\rm Im}\left\{H_t\left(\omega_{i\,\max}\right)\right\}$ so obtained and $\omega_{i\,\max} = 2\pi f_{i\,\max}$ in (7), the following relation between h and $f_{i\,\max}$ can be derived

$$f_{i\,\max} = \frac{V_{\rm dc}}{4\left(L_T + L_s + \left(L_T L_s/L_l\right)\right)h}. \tag{13}$$

For stiff feeder distribution system, i.e., $L_s = 0$, the expression for $f_{i\,\max}$ can be obtained from (13) as

$$f_{i\,\max} = \frac{V_{\rm dc}}{4L_T h}. \tag{14}$$

This expression of the $f_{i\,\max}$ is same as obtained in [11] for the stiff feeder distribution system based on time-domain approach. For the zero input impedance nonlinear load, i.e., $L_l = 0$, (13) results in $f_{i\,\max} = 0$. This implies that the VSI of the compensator cannot track the shunt current, in the absence of L_l. Therefore, input impedance is must for the voltage source type of the load.

Based on the results derived in [18], it can be shown that the instantaneous switching frequency f_i varies twice between the maximum $f_{i\,\max}$ and minimum $f_{i\,\min}$ over one cycle of the fundamental frequency ω_o, as follows:

$$f_i = f_{i\,\max}\left(1 - \left(M_d G\left(\omega_o t + \varphi\right)\right)^2\right) \tag{15}$$

where M_d represents the modulation depth of the inverter and depends upon the system parameters and load of the distribution system. The function $G(\omega_o t + \varphi)$ represents a periodic function with the fundamental frequency of ω_o rad/s. The value of the function is limited between -1 and $+1$. The phase angle φ is defined as the relative position of the zero crossing instant of the error function $e(t)$ at which the maximum switching frequency $f_{i\,\max}$ occurs. For pure reactive power compensation this is a sinusoidal function, i.e., $\sin(\omega_o t + \varphi)$. The minimum switching frequency $f_{i\,\min}$ is a function of the maximum switching frequency $f_{i\,\max}$ and modulation depth M_d and can be obtained from (15) as $f_{i\,\min} = f_{i\,\max}\left(1 - (M_d)^2\right)$.

VI. Single-Phase Shunt Compensation

Load compensation for the single-phase distribution system has been obtained in this section. The load is assumed nonlinear

TABLE I
SYSTEM PARAMETERS FOR THE SINGLE-PHASE DISTRIBUTION SYSTEM AND COMPENSATOR CONSIDERED IN SIMULATIONS

Parameters	*Numerical value*
Source voltage v_s	240.0 V (rms)
System frequency f_o	50 Hz.
Feeder impedance L_s, R_s	1.833 mH, 0.576 Ω
Shunt impedance L_T , R_T	3.67 mH, 0.968 Ω
DC link voltage V_{dc} and capacitor C_{dc}	500.0 V, 4400 μF
Nonlinear load	R_{ldc} = 25.0 Ω, C_{ldc} = 150.0 μF L_{lac} = 3.67 mH, R_{lac} = 0.1152 Ω

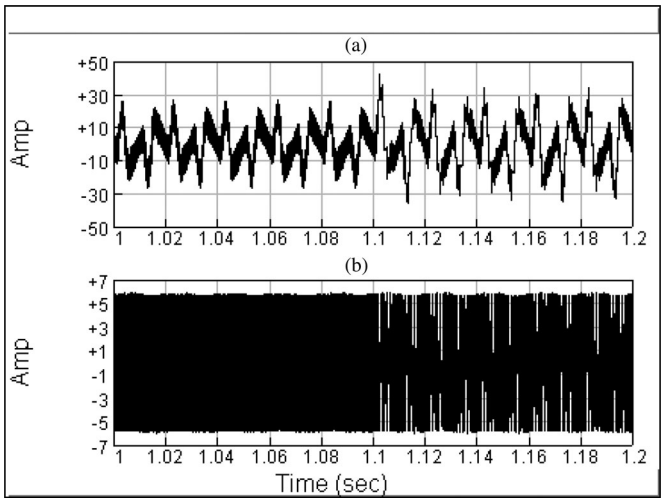

Fig. 5. Hysteresis current controller tracking performance, (a) shunt current and (b) tracking error for weak feeder system.

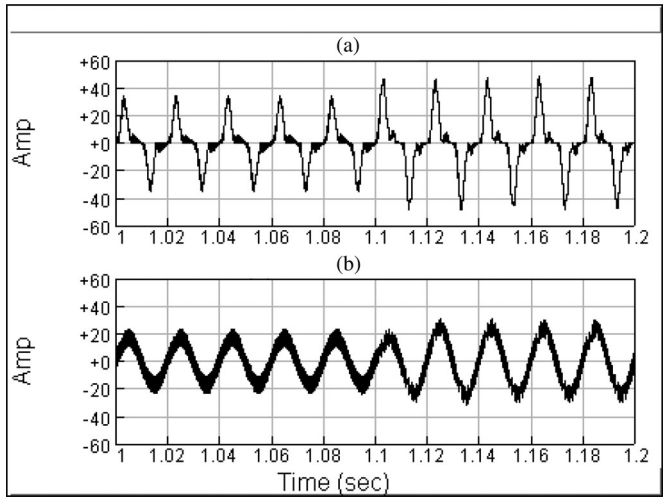

Fig. 6. (a) Load current and (b) source current, for weak feeder distribution system.

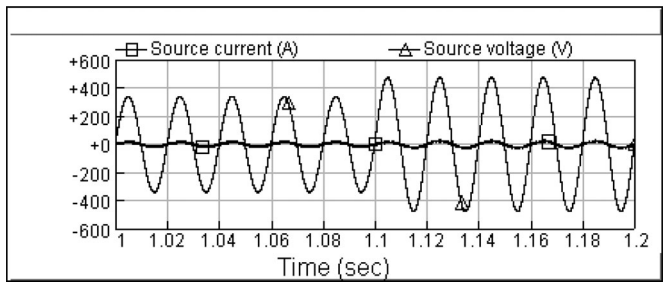

Fig. 7. Source current in phase with the supply voltage for weak feeder system.

that draws both reactive and harmonic components, in addition to the real component. It is desired that the source delivers only the real component of the load while the harmonic and reactive components of the load need to be supplied locally from the shunt compensator.

A. Reference Current Generation for Shunt Compensator

Let the load current i_l shown in Fig. 1 is given by the following expression:

$$i_l = i_{lp} + i_{lq} + i_{lh} \tag{16}$$

where i_{lp}, i_{lq}, and i_{lh} are the real, reactive, and harmonic components of the load current, respectively. It is desired that the compensator injects the shunt current i_{sh} such that it compensates the reactive and harmonic components of the load current. Applying KCL at the PCC in Fig.1, the following relation can be obtained:

$$i_s = i_l - i_{\rm sh}. \tag{17}$$

Now, if the reference for the shunt current $i_{\rm sh}$, in (17) is chosen as follows:

$$i_{\rm shref} = i_{lq} + i_{lh} \tag{18}$$

then the resultant source current i_s would carry only the real component of the load i_{lp}. Following online shunt current reference $i_{\rm shref}$ generation algorithm will ensure that the source delivers only the real component of the load current [32], [33]

$$i_{\rm shref} = i_l - i_{\rm sref} = i_l - \frac{\sqrt{2}\,(p_{\rm lav} + p_{\rm dc})}{(V_{s\rm RMS})} \sin(\omega_o t) \tag{19}$$

where $p_{\rm lav}$ is the average load power that represents the real power drawn by the load, and $V_{s\rm RMS}$ is the RMS value of the supply voltage v_s. The second term in (19) represents the reference current for the source $i_{\rm sref}$ that is same as the real component of the load in (16). When $i_{\rm sref}$ is subtracted from the load current i_l, it ensures that the reference shunt current carries both reactive and harmonic component of the load (18). The sine template $\sin(\omega_o t)$ is phase locked with the filtered component of the locally available supply voltage. The variable $p_{\rm dc}$ in (19) represents the power drawn from the distribution system to replenish the lossses caused by the shunt compensator circuit [32], [33]. The main objective of $p_{\rm dc}$ is to hold the filtered dc-link voltage $V_{\rm dcfil}$ constant equal to the reference dc-link

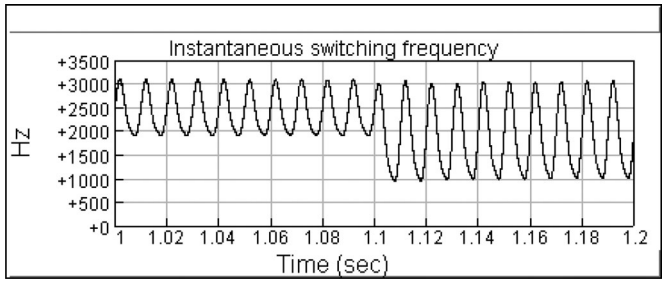

Fig. 8. Variation of instantaneous switching frequency for weak feeder system with $h = 5.6798$ A, the supply voltage rises at 1.1 s.

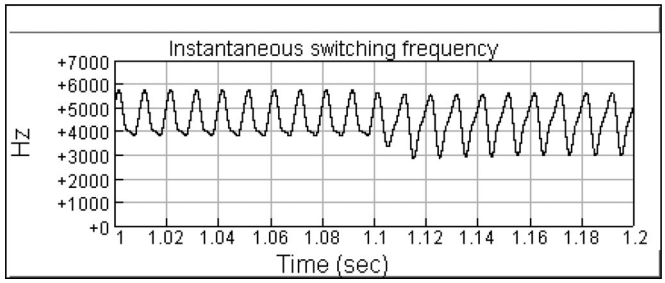

Fig. 10. Variation of instantaneous switching frequency for strong feeder system with $h = 5.6798$ A, the load increases at 1.1 s.

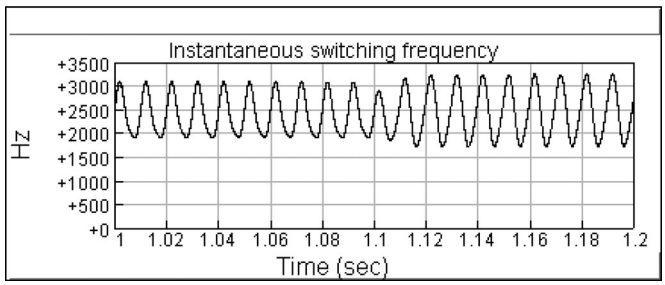

Fig. 9. Variation of instantaneous switching frequency for weak feeder system with $h = 5.6798$ A, the load increases at 1.1 s.

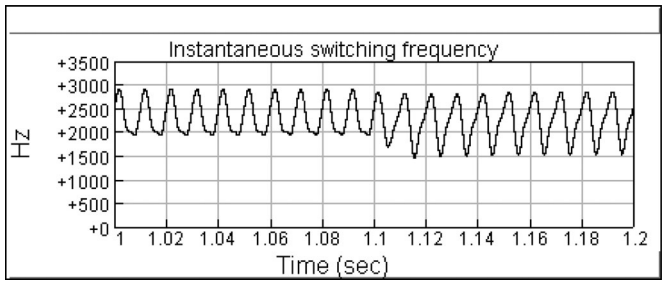

Fig. 11. Variation of instantaneous switching frequency for strong feeder system with $h = 11.3626$ A, the load increases at 1.1 s.

voltage V_{dcref}. The dc control loop is given by

$$p_{\mathrm{dc}} = K_{\mathrm{pdc}} e + K_{\mathrm{idc}} \int e\, dt \tag{20}$$

where K_{pdc} and K_{idc} are the proportional and integral gains, respectively, for the dc control loop and the error e is given as

$$e = V_{\mathrm{dc\,ref}} - V_{\mathrm{dcfilt}}. \tag{21}$$

B. Simulation Results

In this section, the operation of the shunt compensator and verification of the derived results for switching frequency from (13) to (15) have been obtained through the simulation results. Reference current for the shunt compensator is generated using (19). The hysteresis current control algorithm (4) and (5) is used for tracking the reference shunt current.

1) Weak Feeder Distribution System: The data for the weak feeder distribution system and shunt compensator are given in Table I. The calculated value of hysteresis bandwidth from (13) for the chosen maximum switching frequency of $f_{i\ \max} = 3.0$ kHz gives $h = 5.6798$ A. Fig. 5 shows the tracking performance of the hysteresis current controller under steady state. The shunt current is shown in Fig. 5(a) and its tracking error is shown in Fig. 5(b). The error is limited to the hysteresis bandwidth ± 5.6798 A. At $t = 1.1$ s, the supply voltage rises by 40%. The corresponding load and source currents are shown in Fig. 6(a) and (b), respectively. The supply voltage in phase with the resultant source current is shown in Fig. 7. The variation of instantaneous switching frequency f_i is shown in Fig. 8. The dc-link voltage is controlled to the reference 500 V with the values of K_{pdc} and K_{idc} chosen as 0.05 and 0.1 s^{-1}, respectively, in (20). These values of the PI gains have been selected through trial and error for achieving the best dynamic response for dc-link voltage convergence. It is clear from Fig. 8 that the maximum switching frequency of the switching devices used in the single-phase H-bridge inverter is close to 3.0 kHz. However, minimum switching frequency depends upon the modulation depth that in turn depends upon the system conditions. In this case, the reference source current also increases when the supply voltage increases the load current. Hence, the reference shunt current also increases that in turn increases the modulation depth. Therefore, the minimum switching frequency $f_{i\,\min}$ reduces for increase in the supply voltage. Similarly in other simulation, the load is approximately doubled at $t = 1.1$ s, keeping the supply voltage constant. Again as seen from Fig. 9, the maximum switching frequency remains close to 3 kHz, however the minimum reduces when the load increases due to increase in the modulation depth. The detailed result for increase in the load is given in the next section.

2) Strong Feeder Distribution System: It is now assumed that the shunt compensator is used for the load compensation for strong feeder distribution system. All the system parameters are kept same as considered for the weak feeder case earlier, except that the feeder impedance is considered as $L_s = 0, R_s = 0$. With these parameters, the switching frequency gets increased to $f_{i\max} = 6.0$ kHz for the same $h = 5.6798$ A, as calculated from (14). This is also verified from the simulation result as shown in Fig. 10.

In order to bring back the maximum switching frequency to 3.0 kHz, the hysteresis bandwidth is now calculated from (14) for $f_{i\ \max} = 3.0$ kHz as $h = 11.3626$ A. The result for

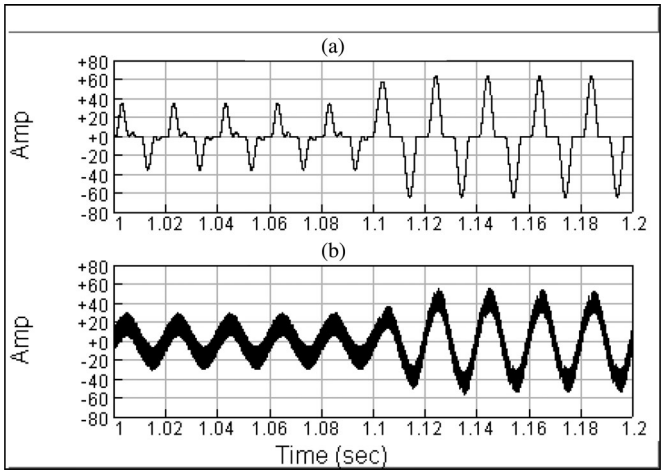

Fig. 12. (a) Load current and (b) source current, for strong feeder system.

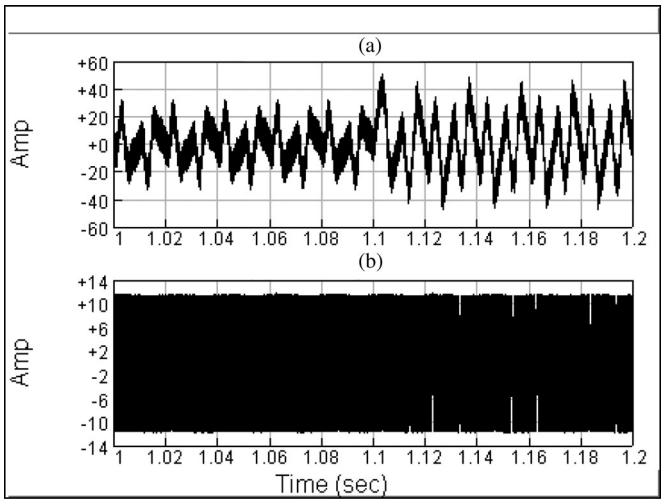

Fig. 13. Hysteresis current controller tracking performance, (a) shunt current and (b) tracking error, for strong feeder system.

instantaneous switching frequency is now verified using the simulation result shown in Fig. 11.

The load is doubled after $t = 1.1$ s as shown in Fig. 12(a). The corresponding source current is shown in Fig. 12(b). With increase in load, the modulation depth of the inverter increases due to increased value of reference shunt current as shown in Fig. 13(a). The tracking error is shown in Fig. 13(b). The maximum switching frequency remains close to 3.0 kHz, however the minimum switching frequency is reduced with increase in load as shown in Fig. 11.

Remark 1: It may be noted from Figs. 8 to 11, that the maximum switching frequency estimation using (13) gives small variation under different operating conditions. This is because the approximated Thevenin's equivalent impedance (L_l, R_l) of the nonlinear load varies with changing conditions of the system and the small variations in the dc-link voltage $V_{\rm dc}$.

TABLE II
SYSTEM PARAMETERS FOR THE SINGLE-PHASE DISTRIBUTION SYSTEM AND COMPENSATOR OF LABORATORY MODEL

Parameters	Numerical value
Source voltage v_s	25.0 V (rms)
System frequency f_o	50 Hz
Feeder impedance L_s, R_s	5.0 mH, 1.0 Ω
Shunt impedance L_T , R_T	10.0 mH, 2.0 Ω
DC link reference voltage V_{dc} and capacitor C_{dc}	50.0 V, 2200 μF
Nonlinear load	R_{ldc} = 25.0 Ω, C_{ldc} = 150.0 μF L_{lac} = 5.0 mH, R_{lac} = 1.0 Ω

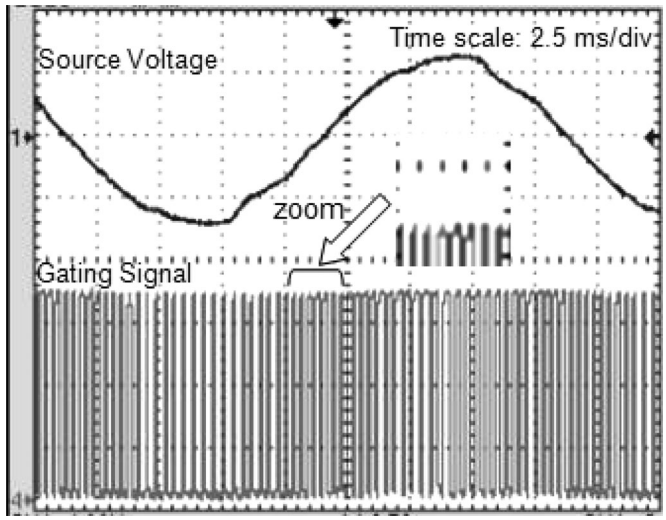

Fig. 14. Normal supply voltage and gating signal for the switches S_{w1} and S_{w2} with the maximum switching frequency of $f_{i\ \max} = 3$ kHz. *Scale:* Source voltage (30 V/div) and gating signal (1 V/div: 0 V-OFF, 3.3 V-ON).

C. Experimental Results

In this section, the experimental results are obtained in a laboratory model of a weak feeder distribution system with the data given in Table II.

In this case, the hysteresis bandwidth of $h = 0.1667$ A is calculated from (13) for $f_{i\ \max} = 3.0$ kHz. The reference current generation and hysteresis current control algorithms have been implemented in PCI-7831R (reconfigurable input/output), field-programmable gate array (FPGA). The VSI is implemented using the IGBT-based intelligent power module (IPM). The load voltage and the load current are feedback using the voltage transducer (LV 25-P) and current transducer (LA 55-P), respectively. These variables are used for the reference current generation and hysteresis current control loop, and are implemented using the LabVIEW FPGA programming module. The reference current $i_{\rm shref}$ generated using (19) is phase locked with the supply voltage at the fundamental frequency using a software-based phase locked loop (PLL) code implemented in the LabVIEW FPGA.

Fig. 14 shows the gating signal generated for the IGBT switches S_{w1} and S_{w2} of the H-bridge shown in Fig. 3 with

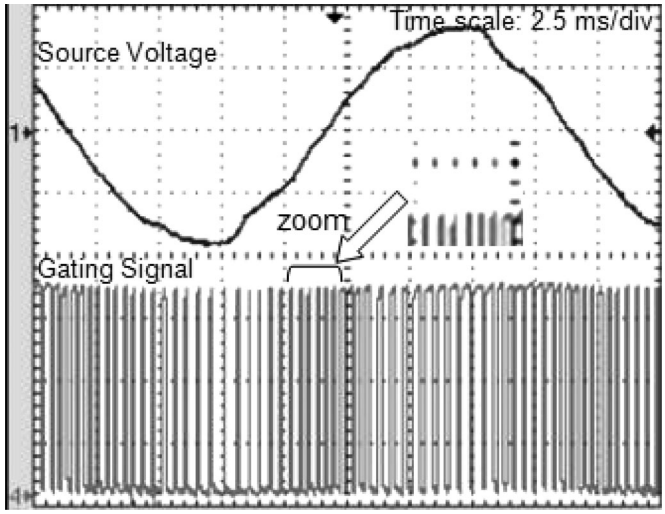

Fig. 15. Rise in supply voltage and gating signal for the switches S_{w1} and S_{w2} with the maximum switching frequency of $f_{i\,\max} = 3$ kHz. *Scale:* Source voltage (30 V/div) and gating signal (1 V/div: 0 V-OFF, 3.3 V-ON).

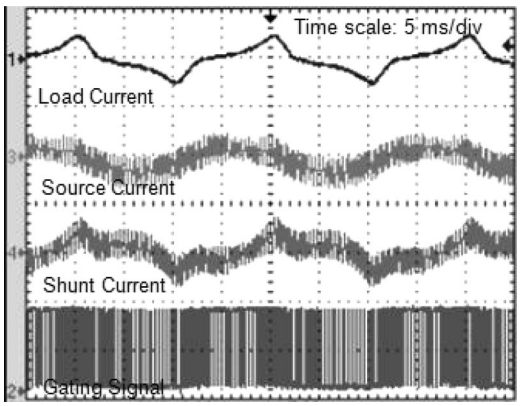

Fig. 16. Load current, source current, injected shunt current, and gating signal for nominal load. *Scale:* Load, source, and shunt currents (5 A/div) and gating signal (2 V/div: 0 V-OFF, 3.3 V-ON).

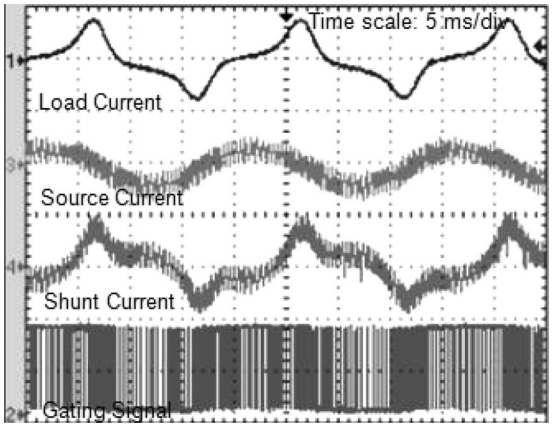

Fig. 17. Load current, source current, injected shunt current, and gating signal for increased load. *Scale:* Load, source, and shunt currents (5 A/div) and gating signal (2 V/div: 0 V-OFF, 3.3 V-ON).

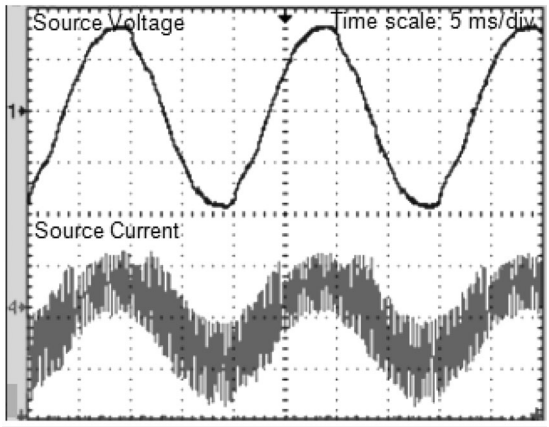

Fig. 18. Source current in phase with the supply voltage. *Scale:* Source voltage (30 V/div) and source current (2 A/div).

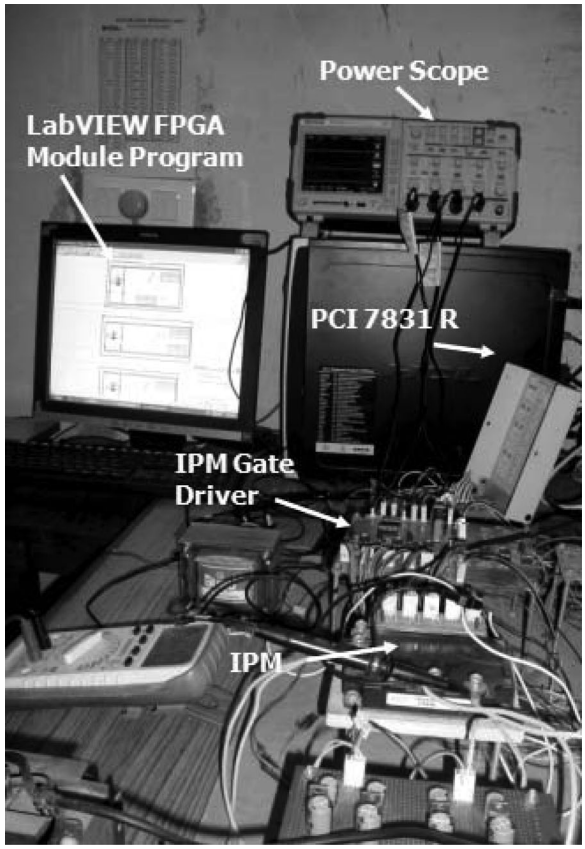

Fig. 19. View of experimental setup showing LabVIEW FPGA controller and VSI of the shunt compensator.

the maximum switching frequency $f_{i\,\max}$ close to 3.0 kHz. This can be easily calculated from the zoomed view of one division of the time scale in Fig. 14, where the switching frequency is maximum, i.e., $f_{i\,\max}$ ($\approx$ number of pulses/time duration $= 7.5/0.0025 = 3000$ Hz). The hysteresis bandwidth of $h = 0.1667$ A is used as calculated earlier. The gating signals for the IGBT switches S_{w3} and S_{w4} are complementary to that shown in Fig. 14. The normal supply (source) voltage is also shown in Fig. 14. The source voltage is line supply voltage and

is distorted as shown in the figure. Similar results for rise in supply voltage are shown in Fig. 15. The maximum switching frequency in this case also is the same, i.e., $f_{i\max}$ is close to 3.0 kHz as seen from zoomed view in Fig. 15. However, the minimum switching frequency for the increased source voltage case is less as compared to the normal supply voltage case. The load current, source current, injected shunt current, and gating signal are shown in Fig. 16 for the case of the load given in Table II. The load is approximately doubled and the corresponding results are shown in Fig. 17. The maximum switching frequency is maintained close to 3.0 kHz, however minimum reduces when the load increases. The source current in phase with the supply voltage is shown in Fig. 18. The dc-link voltage is controlled to the reference 50.0 V.

The experimental result verifies the switching formulation derived in this paper. For the case of strong feeder, the results similar to those shown in Figs. 15–18 can be obtained for the hysteresis bandwidth of $h = 0.4166$ A, as calculated from (14).

Fig. 19 shows a view of the laboratory experimental setup showing the LabVIEW-based FPGA controller used for driving the VSI of the shunt compensator.

VII. Conclusion

The generalized frequency domain method of the switching frequency formulation using a high-frequency model based on Tsypkin's method accurately estimates the hysteresis bandwidth for a desired maximum switching frequency for load compensation using hysteresis current controlled VSI. It is shown that the feeder reactance and load has a significant effect in determining the maximum switching frequency for the weak feeder distribution systems. However, the maximum switching frequency is mainly dependent upon the shunt compensator parameters for strong feeder distribution systems. The minimum switching frequency in general depends upon the modulation depth of the VSI. Results have been verified through detailed simulation studies. The experiment carried on the weak feeder distribution system model verifies the generalized formulation of the switching frequency proposed in this paper.

Acknowledgment

The author would like to thank his Master's students who helped in setting up the experimental model. He is also grateful to Prof. A. Ghosh of Queensland University of Technology, Brisbane, Australia, for his inspirations.

References

[1] J. A. Sayago, T. Brückner, and S. Bernet, "How to select the system voltage of MV drives—A comparison of semiconductor expenses," *IEEE Trans. Ind. Electron.*, vol. 55, no. 9, pp. 3881–3890, Sep. 2008.

[2] H. Baumann, P. Heinemeyer, W. Staiger, M. Töpfer, K. Unger, and D. Müller, "Optimized cooling systems for high-power semiconductor devices," *IEEE Trans. Ind. Electron.*, vol. 48, no. 2, pp. 298–306, Apr. 2001.

[3] D. M. Brod and D. M. Novotny, "Current control of VSI-PWM inverters," *IEEE Trans. Ind. Appl.*, vol. IA-21, no. 4, pp. 562–570, May/Jun. 1985.

[4] J. Holtz, "Pulsewidth modulation—A survey," *IEEE Trans. Ind. Electron.*, vol. 39, no. 5, pp. 410–420, Dec. 1992.

[5] M. P Kazmierkowski and L. Malesani, "Current control techniques for three-phase voltage source PWM converters: A survey," *IEEE Trans. Ind. Electron.*, vol. 45, no. 5, pp. 691–703, Oct. 1998.

[6] S. Buso, L. Malesani, and P. Mattavelli, "Comparison of current control techniques for active filter applications," *IEEE Trans. Ind. Electron.*, vol. 45, no. 5, pp. 722–729, Oct. 1998.

[7] R. Gupta and A. Ghosh, "Frequency-domain characterization of sliding mode control of an inverter used in DSTATCOM application," *IEEE Trans. Circuits. Systs.-I: Reg. Papers*, vol. 53, no. 3, pp. 662–676, Mar. 2006.

[8] M. Mohseni and S. M. Islam, "A New vector-based hysteresis current control scheme for three-phase PWM voltage-source inverters," *IEEE Trans. Power Electron.*, vol. 25, no. 9, pp. 2299–2309, Sep. 2010.

[9] X. Mao, R. Ayyanar, and H. K. Krishnamurthy, "Optimal variable switching frequency scheme for reducing switching loss in single-phase inverters based on time-domain ripple analysis," *IEEE Trans. Power Electron.*, vol. 24, no. 4, pp. 991–1001, Apr. 2009.

[10] Z. Yao, L. Xiao, and Y. Yan, "Dual-buck full-bridge inverter with hysteresis current control," *IEEE Trans. Ind. Electron.*, vol. 56, no. 8, pp. 3153–3160, Aug. 2009.

[11] M. K. Mishra and K. Karthikeyan, "An investigation on design and switching dynamics of a voltage source inverter to compensate unbalanced and nonlinear loads," *IEEE Trans. Ind. Electron.*, vol. 56, no. 8, pp. 2802–2810, Aug. 2009.

[12] A. Z. Albanna and C. J. Hatziadoniu, "Harmonic modeling of hysteresis inverters in frequency domain," *IEEE Trans. Power Electron.*, vol. 25, no. 5, pp. 1110–1114, May 2010.

[13] C. N. M. Ho, V. S. P. Cheung, and H. S. H. Chung, "Constant-frequency hysteresis current control of grid-connected VSI without bandwidth control," *IEEE Trans. Power Electron.*, vol. 24, no. 11, pp. 2484–2495, Nov. 2009.

[14] V. George and M. K. Mishra, "Design and analysis of user-defined constant switching frequency current-control-based four-leg DSTATCOM," *IEEE Trans. Power Electron.*, vol. 24, no. 9, pp. 2148–2158, Sep. 2009.

[15] N. Prabhakar and M. K. Mishra, "Dynamic hysteresis current control to minimize switching for three-phase four-leg VSI topology to compensate nonlinear load," *IEEE Trans. Power Electron.*, vol. 25, no. 8, pp. 1935–1942, Aug. 2010.

[16] B. K. Bose, "An adaptive hysteresis-band current control technique of a voltage-fed PWM inverter for machine drive system," *IEEE Trans. Ind. Electron.*, vol. 37, no. 5, pp. 402–408, Oct. 1990.

[17] M. Kale and E. Ozdemir, "An adaptive hysteresis band current controller for shunt active power filter," *Elec. Power Syst. Res.*, vol. 73, no. 2, pp. 113–119, Feb. 2005.

[18] Q. Yao and D. G. Holmes, "A simple, novel method for variable-hysteresis-band current control of a three phase inverter with constant switching frequency," in *Proc. IEEE Ind. Appl. Soc. Ann. Meet.*, Oct.2–8, 1993, vol. 2, pp. 1122–1129.

[19] R. Gupta, A. Ghosh, and A. Joshi, "Control of cascaded transformer multilevel inverter based DSTATCOM," *Elec. Power Syst. Res.*, vol. 77, no. 8, pp. 989–999, Jun. 2007.

[20] R. Gupta, A. Ghosh, and A. Joshi, "Multi-band hysteresis modulation and switching characterization for sliding mode controlled cascaded multilevel Inverter," *IEEE Trans. Ind. Electron.*, vol. 57, no. 7, pp. 2344–2353, Jul. 2010.

[21] A. Bergen, "A note on Tsypkin's locus," *IRE Trans. Automat. Control*, vol. 7, no. 3, pp. 78–80, Apr. 1962.

[22] Gelb and W. E. Vander Veido, *Multiple-Input Describing Function and Nonlinear System Design*. NY, St. Louis: Mc Graw-Hill, 1968.

[23] D. P. Atherton, *Nonlinear Control Engineering*. Workingham, U.K.: Van Nostrand, 1975.

[24] R. Gupta, A. Ghosh, and A. Joshi, "Cascaded multilevel control of DSTATCOM using multiband hysteresis modulation," in *Proc. IEEE Power Eng. Soc. (PES) General Meeting 2006*, Jun.18–22, 2006.

[25] A. Shukla, A. Ghosh, and A. Joshi, "Hysteresis modulation of multilevel inverters," *IEEE Trans. Power Electron.*, vol. 26, no. 5, pp. 1396–1409, May 2011.

[26] M. Mohseni, S. M. Islam, and M. A. S. Masoum, "Enhanced hysteresis-based current regulators in vector control of DFIG wind turbines," *IEEE Trans. Power Electron.*, vol. 26, no. 1, pp. 223–234, Jan. 2011.

[27] R. Gupta, A. Ghosh, and A. Joshi, "Characteristic analysis for multisampled digital implementation of fixed-switching-frequency closed-loop modulation of voltage-source inverter," *IEEE Trans. Ind. Electron.*, vol. 56, no. 7, pp. 2382–2392, Jul. 2009.

[28] F. Z. Peng, "Application issues of active power filters," *IEEE Ind. Appl. Mag.*, vol. 4, no. 5, pp. 21–30, Sept./Oct. 1998.
[29] S. Rahmani, A. Hamadi, N. Mendalek, and K. Al-Haddad, "A new control technique for three-phase shunt hybrid power filter," *IEEE Trans. Ind. Electron.*, vol. 56, no. 8, pp. 2904–2915, Aug. 2009.
[30] S. C. Y. Chung and L. C. Liang, "A transformed Lure problem for sliding mode control and chattering reduction," *IEEE Trans. Autom. Control*, vol. 44, no. 3, pp. 563–568, Mar. 1999.
[31] E. W. Weisstein, *Pi Formulas,* MathWorld-A Wolfram Web Resource. [Online]. Available: mathworld.wolfram.com/PiFormulas.html
[32] A. Ghosh and G. Ledwich, *Power Quality Enhancement Using Custom Power Devices*. Boston, MA: Kluwer, 2002.
[33] R. S. Herrera and P. Salmerón, "Instantaneous reactive power theory: A reference in the nonlinear loads compensation," *IEEE Trans. Ind. Electron.*, vol. 56, no. 6, pp. 2015–2022, Jun. 2009.

Rajesh Gupta (S'05–M'08–SM'11) received the Bachelor's degree from the Madan Mohan Malviya Engineering College, Gorakhpur, India, in 1993, the Master's degree from the Birla Institute of Technology, Ranchi, India, in 1995, and the Ph.D. degree from the Indian Institute of Technology, Kanpur, India, in 2007, all in electrical engineering.

From 1996 to 1999, he was a Lecturer with the Govind Ballabh Pant Engineering College, Pauri Garhwal, India. He is currently an Associate Professor with the Department of Electrical Engineering, Motilal Nehru National Institute of Technology, Allahabad, India. His research interests include control theory, power electronics systems & control, multilevel converters, power quality, and distributed generation.

Dr. Gupta is a regular reviewer for IEEE TRANSCATIONS ON POWER ELECTRONICS, IEEE TRANSCATIONS ON INDUSTRIAL ELECTRONICS, and *IET Power Electronics*. He volunteered as a Joint Secretary of the IEEE Uttar Pradesh Section for the year 2011 and as Secretary of the IEEE Joint Society Chapter of IE/PEL/CS for the year 2010.